Hindawi Publishing Corporation
Advances in Physical Chemistry
Volume 2015, Article ID 102583, 9 pages
http://dx.doi.org/10.1155/2015/102583

Research Article

Revisiting Oxidative Dehydrogenation of Ethane by W Doping into MoVMn Mixed Oxides at Low Temperature

Mohammed H. Al-Hazmi,[1] Taiwo Odedairo,[1,2] Adel S. Al-Dossari,[1] and YongMan Choi[1]

[1]*SABIC Technology Center, Riyadh 11551, Saudi Arabia*
[2]*School of Chemical Engineering, The University of Queensland, St. Lucia, Brisbane, QLD 4072, Australia*

Correspondence should be addressed to Mohammed H. Al-Hazmi; hazmimh@sabic.com and YongMan Choi; choiy@sabic.com

Received 9 November 2014; Revised 17 December 2014; Accepted 31 December 2014

Academic Editor: Jinlong Gong

The catalytic performance of MoVMnW mixed oxides was investigated in the oxidative dehydrogenation of ethane at three different reaction temperatures (235, 255, and 275°C) using oxygen as an oxidant. The catalysts were characterized by using X-ray diffraction, temperature-programmed reduction, and scanning electron microscopy. The MoVMnW mixed oxide catalyst showed the 70–90% of ethylene selectivity at the reaction temperatures. However, a significant decrease in the selectivity of ethylene was observed by increasing the reaction temperature from 235°C to 275°C.

1. Introduction

Ethylene (C_2H_4) is an important building block used in the petrochemical industry [1]. Its primary production method is the energy-intensive steam cracking process [2] which is usually carried out at $T > 800^{\circ}C$ [3]. Over 100 million metric tons of ethylene is produced annually by means of the steam cracking of long carbon-chain hydrocarbons. In addition to the high energy cost, unavoidable side reactions and the deactivation of catalysts by carbon deposition are other technical shortcomings of the process. Increasing attention has been directed towards the oxidative dehydrogenation (ODH) of alkanes because of its potential benefit of using abundant and inexpensive raw materials [4–6]. The ODH of light alkanes offers a potentially attractive route to alkenes since the reaction is exothermic [2] and avoids the thermodynamic constraints of nonoxidative routes by forming by-product water [7]. However, a low yield and selectivity of olefins still retard the industrial application of the ODH. To date, about a 20% yield of ethylene was reported in the literature, and for industrial applications, it requires the ethylene productivity of above 1 $kg_{C_2H_4}/kg_{cat}^{-1}\,h^{-1}$ [8]. The ODH of ethane to ethylene has received less attention than the nonoxidative cracking [9]. However, ethane is the second-largest component of natural gas and the primary product of the methane conversion by oxidative coupling. Thus, a large number of catalysts have been investigated for the ODH of ethane and propane, for example, using Mo-V based catalysts [10–13]. It was reported that a V based catalyst is one of the most active and selective single metal catalysts in the ODH [14, 15], while V [10, 16–18], Mo [12, 13, 19–21], Pt [22–25] based catalysts, and MoV mixed oxides [26–28] are the most widely studied transition-metal catalysts for the ODH of ethane. Furthermore, a more complicated material (i.e., $Mo_1V_{0.25}Nb_{0.12}Pd_{0.0005}O_x$ [29–31]) with two different catalytic centers, such as the ODH of ethane and the heterogeneous Wacker oxidation of ethylene to acetic acid, was reported. The catalytic activity of MoV based catalysts supported on TiO_2 and Al_2O_3 was investigated in the ODH of both ethane and propane [32]. Recently, the catalytic properties of the acidic and basic forms of Ni-, Cu-, and Fe-loaded Y zeolites were investigated in the ODH of ethane to ethylene [33]. As discussed above, although numerous studies on the ODH of ethane using MoV based mixed oxides were reported [29, 31, 32, 34, 35], to the best of our knowledge, little studies using W doping into MoV mixed oxide catalysts have been reported in the literature [35, 36], demonstrating the ethane conversion is the best using a 6.3 mol% W doping to MoVMn mixed oxide catalysts. In this study, to obtain a more systematic, optimal condition of MoVMnW based catalysts

for the ODH of ethane, we investigated the effect of various reaction conditions (i.e., contact time, reaction temperature, and conversion) on the selectivities of ethylene, acetic acid, and CO_x.

2. Experimental

2.1. Catalyst Preparation. As mentioned, 6.3 mol% of W doping to MoVMn mixed oxide catalysts showed the best conversion of ethane by the ODH [35]. Based on the previous study, we applied three materials of $MoV_{0.4}Mn_{0.18}W_0O_x$ (W_0), $MoV_{0.4}Mn_{0.18}W_{0.063}O_x$ ($W_{0.06}$), and $MoV_{0.4}Mn_{0.18}W_{0.14}O_x$ ($W_{0.14}$). We considered W_0 and $W_{0.14}$ as the extreme cases without W and the highest doping, respectively, and $W_{0.06}$ as the optimal one in terms of the ethane conversion from the ODH. The synthesis method is described in detail elsewhere [36]. Briefly, ammonium metavanadate (Fluka Chemical) was added to deionized water and heated to 85°C, with a constant stirring. A yellow colored solution was obtained. Oxalic acid (Riedel-de Haën Chemicals) was added with water to the solution with constant stirring, while the required amount of ammonium tungstate (BDH Chemicals) and manganese acetate (Riedel-de Haën Chemicals, resp.) was slowly added to the mixture. Then, ammonium heptamolybdate (Riedel-de Haën Chemicals) was added to the solution. Precipitates were dried in an oven at 120°C and calcined at 350°C for 4 hours. The calcined catalysts were screened into uniform particles of a 40/60 mesh.

2.2. Characterization of Catalysts. The samples were characterized using several characterization tools including X-ray diffraction (XRD). It was recorded on a Mac Science MX18XHF-SRA powder diffractometer with monochromatized Cu Kα radiation (λ = 0.154 nm) at 40 kV and 30 mA. A Micromeritics AutoChem II 2920 with a thermal conductivity detector (TCD) was used for the H_2 temperature-programmed reduction (TPR) analysis to study the reduction properties of the samples. 15–20 mg of the catalyst samples was heated from 40°C to 1000°C at a heating rate of 10°C/min in 10% H_2 in Ar. Before the H_2-TPR analysis, the samples were heated for 60 min in Ar flow at 100°C. The profile of consumed H_2 was recorded by the TCD. Scanning electron microscopy (SEM) images were recorded using a JEOL JSM-5500LV. Surface area calculations were carried out using The Brunauer-Emmett-Teller (BET) method. Adsorption isotherms were measured in Quantachrome AUTO-SORB-1 at −196°C.

2.3. Reaction Apparatus and Procedures. Catalytic experiments were carried out in a fixed-bed reactor (I.D. = 0.78 cm) with the contact times of 0.08, 0.12, 0.16, 0.24, 0.32, 0.49, and 0.65 sec. The contact time was changed by varying the weight of the catalyst in the range of 50–400 mg and at a total flow of 30 mL/min. All experiments were carried out at 235, 255, and 275°C and at 200 psi. The gas feed composition used in this study was fixed at 15 vol.% ethane in 85 vol.% air. To avoid any mass resistance problem of feed, the prepared powder was pressed to pellets, then crushed, and sieved to 40–60 mesh particles. Reactants and products were analyzed using an online gas chromatograph equipped with a double detector (i.e., thermal conductivity detector (TCD) and flame ionization detector (FID)) and two columns of HayeSep D 80/100 mesh and LAC446. We confirmed the reproducibility of the experiment results within the uncertainty of ±2%. Then, we obtained the conversion (X_{ethane}), selectivity to product i (S_i), and yield to product i (Y_i).

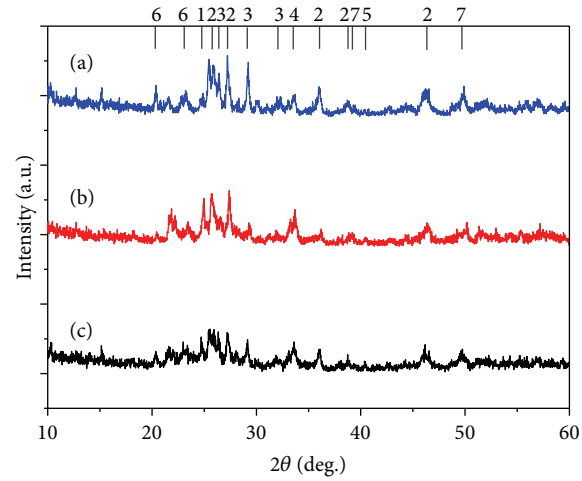

FIGURE 1: XRD patterns of (a) W_0, (b) $W_{0.06}$, and (c) $W_{0.14}$ calcined at 400°C. The numbers (1, 2, 3, 4, 5, 6, and 7) on the top x-axis correspond to WO_3 or WO_4, MoO_3, Mo suboxide such as Mo_8O_{23} or Mo_9O_{26}, $(M_xMo_{1-x})_5O_{14}$ (M = V or Mn or W), W_3O, $V_{0.95}Mo_{0.97}O_5$, and Mn_2O_3, respectively.

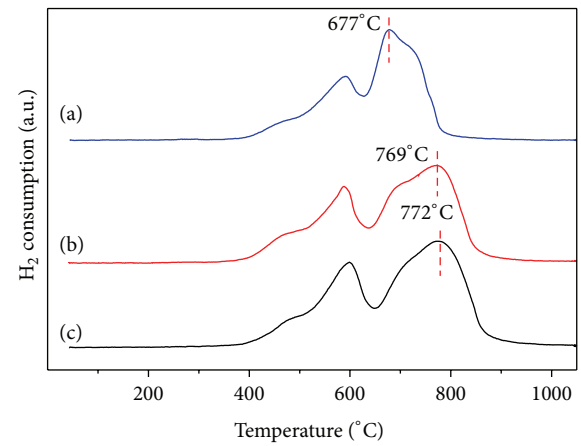

FIGURE 2: H_2-TPR profiles of (a) W_0, (b) $W_{0.06}$, and (c) $W_{0.14}$ catalysts. The dashed lines are the reduction peaks.

3. Results and Discussion

3.1. Characterization of Samples. Crystalline phases of the three catalysts were characterized by XRD. Figure 1 shows XRD patterns of W_0, $W_{0.06}$, and $W_{0.14}$ calcined at 400°C. Mo suboxides (i.e., Mo_8O_{23} (or Mo_9O_{26}), MoO_3, and $(V_xMo_{1-x})_5O_{14}$) were noticed as the major phases (Figure 1).

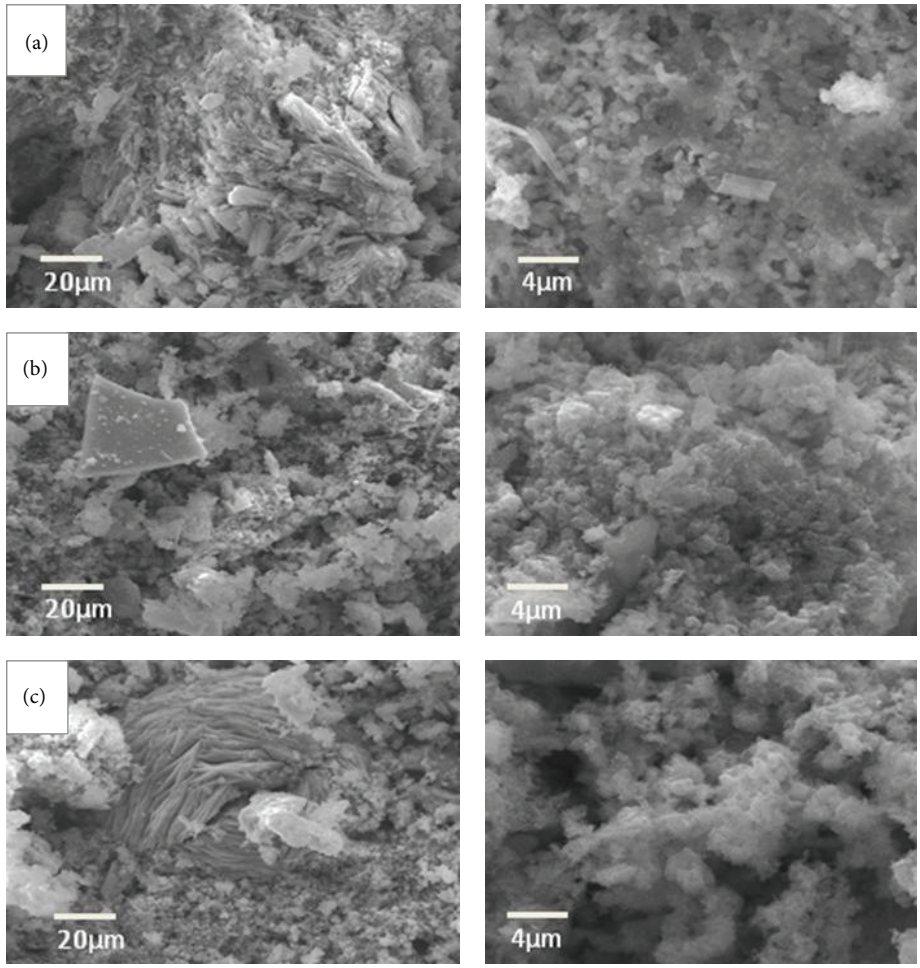

Figure 3: SEM images of (a) W_0, (b) $W_{0.06}$, and (c) $W_{0.14}$.

Also, $(M_xMo_{1-x})_5O_{14}$ (M = V, Mn, or W) was observed as one of the major phases. The reason that most lines of MoO_3 are shifted compared to the standard pattern (JCPDS 76-1003) may be due to a modification by vanadium (i.e., orthorhombic α-$V_xMo_{1-x}O_{3-0.5x}$) or the formation of oxygen vacancies in MoO_{3-x}. Also, triclinic $V_{0.95}Mo_{0.97}O_5$ (JCPDS 77-0649), whose XRD patterns are close to that proposed for VMo_3O_{11} [37], was observed. The BET surface areas of W_0, $W_{0.06}$, and $W_{0.14}$ are 15.6 m^2/g, 13.9, and 15.3, respectively, indicating that the W doping shows an insignificant effort on the textural properties of the materials.

TPR in H_2 was performed to examine reduction characteristics of the mixed oxide catalysts as displayed in Figure 2. There are two reduction peaks observed for W_0 at 587°C and 677°C which correspond to the reduction of isolated V^{5+} species in the bulk structure of the catalyst [38, 39] and Mo^{6+} species [40], respectively. In addition, the observed shoulder at a temperature around 470°C is assumed to be H_2 uptake associated with the reduction of MnO_2 to Mn_2O_3 [41]. The position of the peak at 677°C is shifted to higher temperatures of 769°C ($W_{0.06}$) and 772°C ($W_{0.14}$) and becomes broadened without a significant change in peak intensities. Solsona and coworkers [42] reported a similar shift when W was added to NiO and proposed that the shift was related to an interaction between NiO and tungsten oxide nanoparticles. As shown in the peaks of $W_{0.06}$, the H_2 consumption at 470°C and 587°C was enhanced by the addition of W loading (W_0 versus $W_{0.06}$). We observed that the reduction occurred slightly at higher temperatures by adding more W into the MoVMn based catalysts ($W_{0.06}$ versus $W_{0.14}$).

Figure 3 shows typical SEM images of W_0, $W_{0.06}$, and $W_{0.14}$ doped catalysts, displaying that all samples have irregular shaped particles. The SEM image of W_0 without W ascertains a rough surface with variable shapes and sizes, and a few regions show a stack of fine crystallites (Figure 3(a)). Similarly, $W_{0.06}$ has a rough surface with variable shapes and sizes, but without a stack of fine crystallites (Figure 3(b)). The SEM images of $W_{0.14}$ determine a stack of fine crystallites, leading to a flower-like morphology (Figure 3(c)).

3.2. Catalytic Performance from the ODH of Ethane. Figure 4 shows the effect of W loading on the ethane conversion and product selectivity from the ODH of ethane at 275°C and at a reaction time of 0.65 sec. Ethylene is observed as the major product from the ODH of ethane, while acetic acid, CO, and CO_2 are also detected. The highest ethane

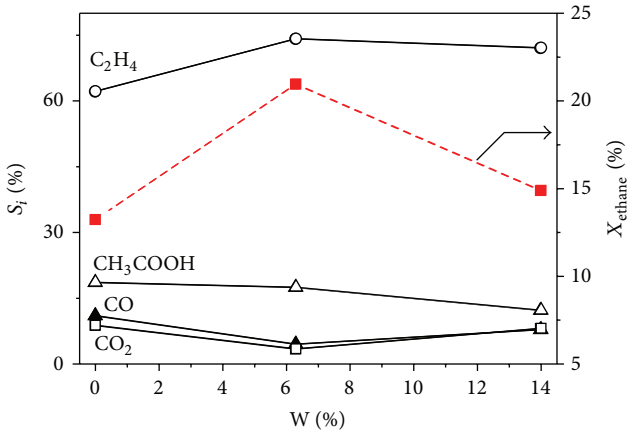

FIGURE 4: Influence of W loading into MoVMn mixed oxide samples at 275°C and at a reaction time of 0.65 sec.

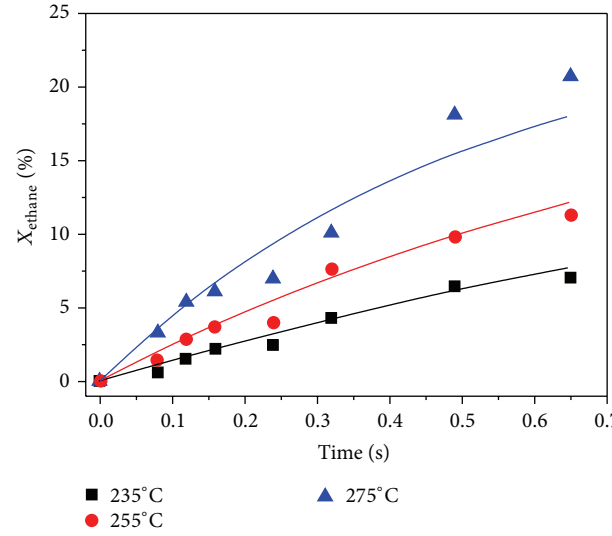

FIGURE 5: Variation of ethane conversion against contact time achieved over the $W_{0.06}$ catalyst at 235 (■), 255 (●), and 275°C (▲). The solid curves are predicted results based on the kinetic modeling.

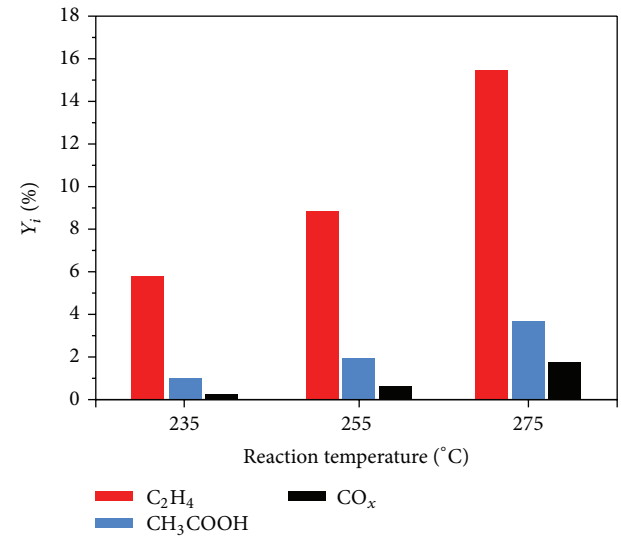

FIGURE 6: Yield from the OHD of ethane over the $W_{0.06}$ catalyst (reaction temperatures = 235, 255, and 275°C and a contact time = 0.65 sec).

conversion (~21.0%) is observed from the MoVMn sample with W = 0.063. The increase in the amount of W over the MoVMn sample leads to a reduction in the conversion of ethane. Similarly, the addition of W results in an increase in the selectivity of ethylene with a maximum selectivity (~74%) achieved at W = 0.063. The lowest selectivity of acetic acid (~12%) is detected at W = 0.14. The ODH experiment of ethane was carried out at two more temperatures of 235 and 255°C using the $W_{0.06}$ catalyst with the contact times of 0.08, 0.12, 0.16, 0.24, 0.32, 0.49, and 0.65 sec (Figure 5). As shown in Figure 5, ethane conversions of approximately 7.0, 11.3, and 21.0% are achieved at 235, 255, and 275°C, respectively, at a contact time of 0.65 sec. The conversion of ethane is improved as the contact time increases. In this study, the maximum ethane conversion was obtained at 275°C. The product distribution from the ODH of ethane on the $W_{0.06}$ catalyst at 235, 255, and 275°C is presented in Figure 6. At all temperatures studied, ethylene is the major product, while acetic acid and carbon oxides are also observed (i.e., ~3.5% and ~1.7%, resp., at 275°C). Figure 7 presents the influence of reaction temperatures and contact times for the selectivities of ethylene, acetic acid, and carbon oxides (CO and CO_2). The selectivities of ethylene decrease by the increase of contact times at all temperatures studied. The highest selectivity of ethylene is observed at a reaction temperature of 235°C. Increasing the reaction temperature from 235°C to 275°C leads to a reduction in the selectivity of ethylene, while an enhancement of selectivities of acetic acid, CO, and CO_2 are observed (Figure 7(b) and Table 1). Table 1 compiles theoretical selectivities of ethylene and CO_x at each reaction temperature. The trend of the reaction products over the $W_{0.06}$ catalyst indicates that ethylene is a key source of acetic acid and carbon oxides. Furthermore, the reduction of the selectivity of ethylene along with the corresponding increase of the by-products (acetic acid and carbon oxides) clearly manifests that acetic acid and carbon oxides are the secondary products from the consecutive oxidation of ethylene. The effect of ethane conversion on the selectivities of ethylene, acetic acid, CO, and CO_2 at 235, 255, and 275°C over $W_{0.06}$ is plotted in Figure 8, demonstrating a strong dependence of ethane conversion and selectivity. It is observed that the selectivity decreases as ethane conversion increases. Also, the selectivity of by-products (i.e., acetic acid, CO_2, and CO) shows a linear relation with the conversion of ethane. As the reaction temperature increases, the selectivity of ethylene decreases. Our experimental data suggest that ethylene undergoes substantial further oxidation, and the ODH of ethane can be described by the parallel consecutive scheme [43].

3.3. Kinetic Studies. A kinetic model was developed to understand the ODH of ethane on MoVMnW mixed oxide catalysts. A generally accepted scheme for the ODH of ethane

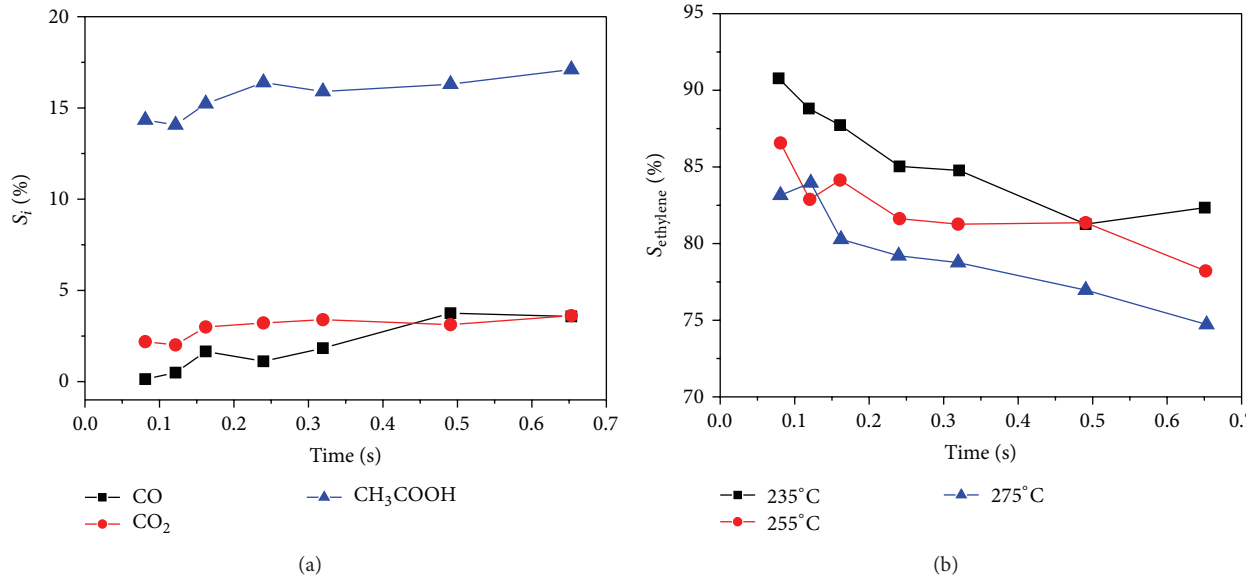

FIGURE 7: Contact-time dependence of selectivities for (a) CH_3COOH, CO, and CO_2 at 275°C and (b) ethylene at 235, 255, and 275°C in the ODH of ethane over the $W_{0.06}$ catalyst.

TABLE 1: Theoretical selectivities[a] of ethylene and CO_x.

Reaction temperature (°C)	$S_{ethylene}$ (%)	S_{CO_x} (%)
235	90.5	1.4
255	85.9	2.0
275	84.0	1.9

[a]They were obtained by linear regression analyses at their zero conversion.

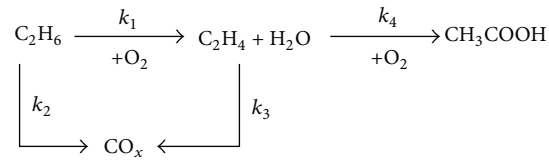

SCHEME 1: Schematic of catalytic reactions of the ODH of ethane.

is shown in Scheme 1 [3, 33, 44]. The kinetic parameters k_{0i}, E_i, and α for the ODH of ethane over the $W_{0.06}$ catalyst were obtained using a nonlinear regression. To develop a kinetic model for the ODH of ethane, three assumptions were made: (1) the ODH is isothermal, (2) a catalyst deactivation is a function of time-on-stream (TOS), and (3) a single deactivation function is defined for all reactions, and a thermal conversion is neglected. Based on the assumptions, rates of the disappearance of ethane ($r_{C_2H_6}$) and the formation of ethylene ($r_{C_2H_4}$), acetic acid (r_{CH_3COOH}), and carbon oxides (r_{CO_x}), respectively, are described as follows:

$$-\frac{dC_{C_2H_6}}{dt_\tau} = \left(k_1 C_{C_2H_6} C_{O_2} + k_2 C_{C_2H_6} C_{O_2}\right) \cdot \varphi \quad (1)$$

$$\frac{dC_{C_2H_4}}{dt_\tau} = \left(k_1 C_{C_2H_6} C_{O_2} - k_3 C_{C_2H_4} C_{O_2} - k_4 C_{C_2H_4} C_{O_2}\right) \cdot \varphi \quad (2)$$

$$\frac{dC_{CH_3COOH}}{dt_\tau} = \left(k_4 C_{C_2H_4} C_{O_2}\right) \cdot \varphi \quad (3)$$

$$\frac{dC_{CO_x}}{dt_\tau} = \left(k_2 C_{C_2H_6} C_{O_2} + k_3 C_{C_2H_4} C_{O_2}\right) \cdot \varphi, \quad (4)$$

where C_i is a concentration of species i in the units of mol/m^3, t_τ is a reaction in the unit of time (i.e., at inlet of the catalyst bed, $t_\tau = 0$, and at the outlet of the catalyst bed, $t_\tau = \tau$), k_i is an apparent rate constant for the ith reaction in the unit of s^{-1}, and φ is the apparent deactivation function. The measurable variables from our chromatographic analysis are the weight fraction of the species, y_x, in the system. By definition the molar concentration, C_x, of every species in the system can be related to its mass fraction, y_x by the following relation:

$$C_x = \frac{y_x F_{TM}}{\upsilon_o MW_x}, \quad (5)$$

where F_{TM} is the total mass flow rate (kg/min), MW_x is the molecular weight of species x in the system, and υ_o is the total volumetric flow rate (m^3/min).

Regarding catalyst deactivation, as deactivation functions can be expressed in terms of the catalyst time-on-stream ($\varphi = \exp(-\alpha t)$), deactivation can also be related to the progress of the reaction [45], where α is a catalyst deactivation constant. The deactivation function based on time-on-stream was initially suggested by Voorhies [46].

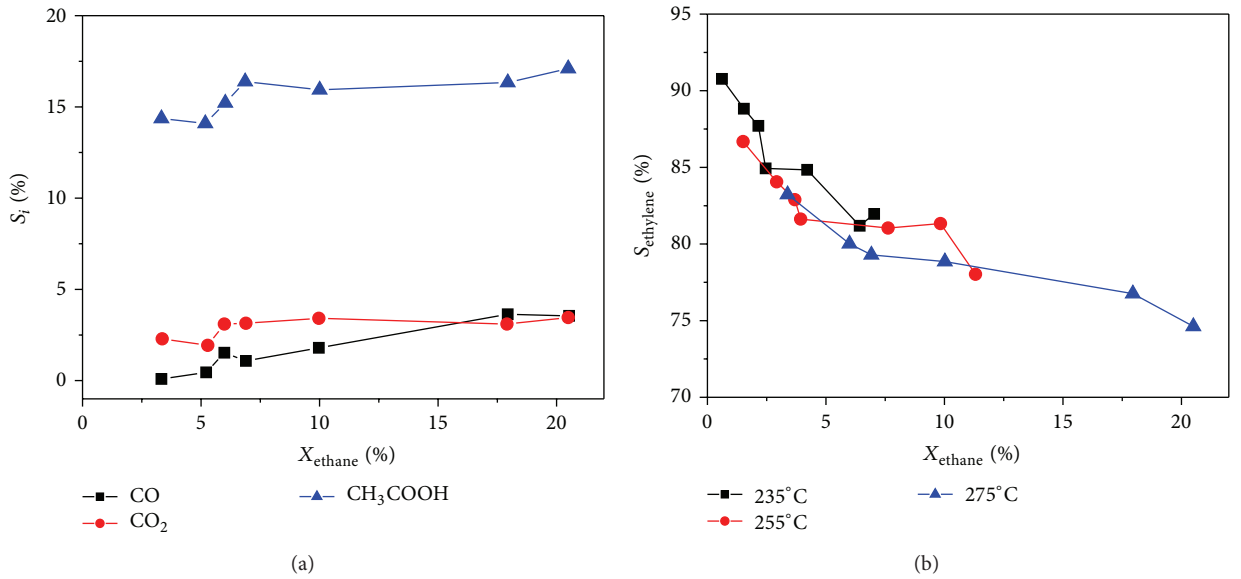

FIGURE 8: Dependence of ethane conversion versus selectivity for (a) CH_3COOH, CO, and CO_2 at 275°C and (b) ethylene at 235, 255, and 275°C in the ODH of ethane over the $W_{0.06}$ catalyst. The data sets are from different contact times.

Substituting (5) into (1)–(4), we have the following first order differential equations which are in terms of weight fractions of the species:

$$-\frac{dy_{C_2H_6}}{dt_\tau} = J_1\left(k_1 y_{C_2H_6} y_{O_2} + k_2 y_{C_2H_6} y_{O_2}\right)\exp(-\alpha t) \quad (6)$$

$$\frac{dy_{C_2H_4}}{dt_\tau} = \left(J_2 k_1 y_{C_2H_6} y_{O_2} - J_1 k_3 y_{C_2H_4} y_{O_2} - J_1 k_4 y_{C_2H_4} y_{O_2}\right) \cdot \exp(-\alpha t) \quad (7)$$

$$\frac{dy_{CH_3COOH}}{dt_\tau} = \left(J_3 k_4 y_{C_2H_4} y_{O_2}\right)\exp(-\alpha t) \quad (8)$$

$$\frac{dy_{CO_x}}{dt_\tau} = \left(J_4 k_2 y_{C_2H_6} y_{O_2} + J_5 k_3 y_{C_2H_4} y_{O_2}\right)\exp(-\alpha t), \quad (9)$$

where J_1, J_2, J_3, J_4, and J_5, respectively, are given by $J_1 = F_{TM}/v_o MW_{O_2}$, $J_2 = F_{TM} MW_{C_2H_4}/v_o MW_{C_2H_6} MW_{O_2}$, $J_3 = F_{TM} MW_{CH_3COOH}/v_o MW_{C_2H_4} MW_{O_2}$, $J_4 = F_{TM} MW_{CO_x}/v_o MW_{C_2H_6} MW_{O_2}$, and $J_5 = F_{TM} MW_{CO_x}/v_o MW_{C_2H_4} MW_{O_2}$. The temperature dependence of the rate constants was represented with the centered temperature form of the Arrhenius equation; that is,

$$k_i = k_{oi}\exp\left[\frac{-E_i}{R}\left(\frac{1}{T} - \frac{1}{T_o}\right)\right], \quad (10)$$

where T_o is an average temperature introduced to reduce parameter interaction in the unit of K [47], k_{oi} is the rate constant for reaction i at T_o (s^{-1}), and E_i is the activation energy for reaction i (kJ/mol). Since the experimental runs were done at 235, 255, and 275°C, T_o was calculated to be 255°C. The values of the model parameters along with their corresponding 95% confidence limits (CLs) are shown in Table 2, while the resulting cross-correlation matrices are also given in Table 3. The cross-correlation matrices give good results as indicated by a low correlation between most of the parameters, with only a few exceptions. From the results of the kinetic parameters presented in Table 2, it was observed that the catalyst deactivation was found to be small, α = 0.03, indicating a low coke formation. As mentioned, the ODH of ethane can occur via the reaction network as shown in Scheme 1, in which ethane reacts with oxygen to form ethylene with a rate constant k_1, or carbon oxides (CO_x) with a rate constant k_2. Ethylene, then, undergoes a subsequent oxidation to CO_x and CH_3COOH with rate constants k_3 and k_4, respectively. Rate constants k_1 and k_2 can be used to determine the ODH of ethane activities, while the ratios of rate constants (i.e., k_1/k_2 and k_1/k_3) are used to determine the ethylene selectivity. High ethylene yields at a reasonable contact time apparently require high values of k_1 and low values of k_2/k_1 and k_3/k_1. The kinetic parameters (k_1, k_2, k_3, and k_4) summarized in Table 2 confirms the high selectivity of ethylene noticed in the ODH of ethane over the $W_{0.06}$ catalyst. Apparent activation energies of 60.5 ± 8.0, 139.6 ± 15.7, 92.4 ± 13.9, and 24.1 ± 2.2 kJ/mol were obtained for the ethane ODH (E_1), ethane combustion (E_2), alkene combustion (E_3), and

TABLE 2: Estimated kinetic parameters for the ODH of ethane on the $W_{0.06}$ catalyst.

Parameters	Values				
	k_1	k_2	k_3	k_4	α
E_i (kJ/mol)	60.5	139.6	92.4	24.1	0.03
95% CL	8.0	15.7	13.9	2.2	
$k_{oi} \times 10^4$ (s^{-1})	0.670	0.045	0.310	0.810	
95% CL × 10^4	0.005	0.016	0.012	0.053	

Table 3: Correlation matrix for the ODH of ethane on the $W_{0.06}$ catalyst.

	k_1	E_1	k_2	E_2	k_3	E_3	k_4	E_4
k_1	1.0000	−0.0418	−0.1419	0.0091	−0.8099	0.6532	−0.8724	0.5709
E_1	−0.0418	1.0000	0.0134	−0.0920	0.2143	−0.4422	0.1922	−0.6074
k_2	−0.1419	0.0134	1.0000	−0.6775	0.1504	−0.1199	0.2001	−0.1467
E_2	0.0091	−0.0920	−0.6775	1.0000	−0.0374	0.0811	−0.0651	0.1535
k_3	−0.8099	0.2143	0.1504	−0.0374	1.0000	−0.9407	0.8263	−0.6696
E_3	0.6532	−0.4422	−0.1199	0.0811	−0.9407	1.0000	−0.7305	0.7559
k_4	−0.8724	0.1922	0.2001	−0.0651	0.8263	−0.7305	1.0000	−0.8308
E_4	0.5709	−0.6074	−0.1467	0.1535	−0.6696	0.7559	−0.8308	1.0000

the formation of CH_3COOH from C_2H_4 (E_4), respectively, following the order of $E_4 < E_1 < E_3 < E_2$. Recently, Lin et al. [33] reported apparent activation energy of ~51.5 kJ/mol for the formation of ethylene over a K-Y zeolite. Similarly, an apparent activation energy (E_1) of ~63.2 kJ/mol was reported for the formation of ethylene over VO_x/SiO_2 catalyst [6]. These values are in good agreement with that calculated over the $W_{0.06}$ catalyst. Argyle and coworkers [7] reported apparent activation energies ~115 kJ/mol and ~60–90 kJ/mol for ethane combustion (E_2) and alkene combustion (E_3), respectively, over an alumina-supported vanadia catalyst. The apparent activation energies obtained for ethane and ethylene combustion to form carbon oxides in this present study show a similar order of magnitude with those reported in the literature. Using the estimated kinetic parameters, we carried out kinetic modeling to examine the validity of the simulated results, and compared them with our experiments finding (i.e., Figures 5 and 9). The fitted parameters were substituted into the comprehensive model developed for this scheme, and the equations were solved numerically by using the 4th-order-Runge-Kutta routine. It was found that our prediction is in good agreement with experiment (Figures 5 and 9), demonstrating the validity of the proposed kinetic model. It is assumed that the slight deviation observed in Figure 9 at 275°C might be due to the significant side products generated at this reaction temperature. It is proposed to carry out microkinetic modeling based on a mechanistic study using density functional theory (DFT) simulations [48, 49], providing more detailed information of the conversion, selectivity, and yield of C_2H_4, CH_3COOH, CO, and CO_2 on W-doped surfaces. The DFT based study would facilitate rationally design of novel MoVMnW mixed oxide catalysts.

4. Conclusions

MoVMnW mixed oxide catalysts were revisited to examine the ODH of ethane. It was found that the addition of W to MoVMn mixed oxide catalysts improves the catalytic activity toward C_2H_4, while lowering the formation of by-products (CH_3COOH, CO, and CO_2). Using the $MoV_{0.4}Mn_{0.18}W_{0.063}O_x$ ($W_{0.06}$) catalyst, we observed that the primary product of ethane oxidation is ethylene, which may go through consecutive reactions to CH_3COOH, CO, and CO_2. The best selectivity of ethylene on the catalyst was ~90% at 235°C. However, a significant decrease in the selectivity of ethylene was observed by increasing the reaction temperature from 235°C to 275°C.

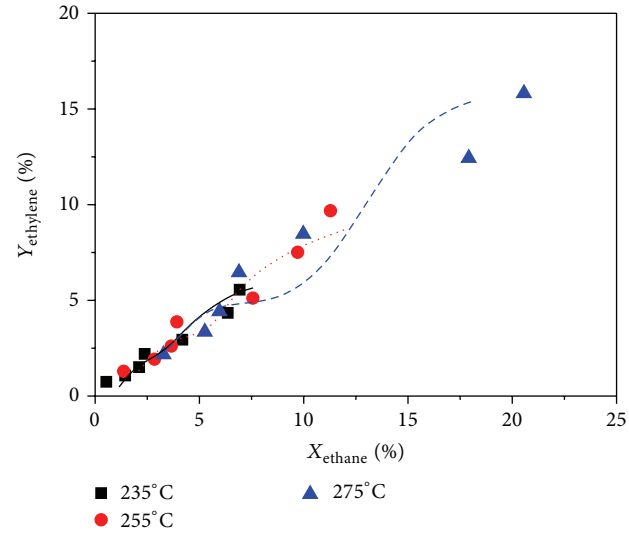

Figure 9: Ethylene yield versus ethane conversion at the reaction temperatures of 235, 255, and 275°C. The solid, dashed, and dotted curves are predicted results based on the kinetic model.

Conflict of Interests

The authors declare that there is no conflict of interests regarding the publication of this paper.

Acknowledgments

The authors highly appreciated the financial support by SABIC. YongMan Choi acknowledges the technical discussion with Professor Ming-Kang Tsai. The authors thank the reviewers' valuable comments, which have improved their paper substantially.

References

[1] S. Seifzadeh Haghighi, M. R. Rahimpour, S. Raeissi, and O. Dehghani, "Investigation of ethylene production in naphtha thermal cracking plant in presence of steam and carbon dioxide," *Chemical Engineering Journal*, vol. 228, pp. 1158–1167, 2013.

[2] C. A. Gärtner, A. C. vanVeen, and J. A. Lercher, "Oxidative dehydrogenation of ethane: common principles and mechanistic aspects," *ChemCatChem*, vol. 5, no. 11, pp. 3196–3217, 2013.

[3] X. Lin, C. A. Hoel, W. M. H. Sachtler, K. R. Poeppelmeier, and E. Weitz, "Oxidative dehydrogenation (ODH) of ethane with O_2 as oxidant on selected transition metal-loaded zeolites," *Journal of Catalysis*, vol. 265, no. 1, pp. 54–62, 2009.

[4] M. L. Rodriguez, D. E. Ardissone, E. Heracleous et al., "Oxidative dehydrogenation of ethane to ethylene in a membrane reactor: a theoretical study," *Catalysis Today*, vol. 157, no. 1–4, pp. 303–309, 2010.

[5] A. Machocki and A. Denis, "Simultaneous oxidative coupling of methane and oxidative dehydrogenation of ethane on the Na^+ /CaO catalyst," *Chemical Engineering Journal*, vol. 90, no. 1-2, pp. 165–172, 2002.

[6] R. Grabowski and J. Słoczyński, "Kinetics of oxidative dehydrogenation of propane and ethane on VO_x/SiO_2 pure and with potassium additive," *Chemical Engineering and Processing: Process Intensification*, vol. 44, no. 10, pp. 1082–1093, 2005.

[7] M. D. Argyle, K. Chen, A. T. Bell, and E. Iglesia, "Effect of catalyst structure on oxidative dehydrogenation of ethane and propane on alumina-supported vanadia," *Journal of Catalysis*, vol. 208, no. 1, pp. 139–149, 2002.

[8] F. Cavani, N. Ballarini, and A. Cericola, "Oxidative dehydrogenation of ethane and propane: how far from commercial implementation?" *Catalysis Today*, vol. 127, no. 1–4, pp. 113–131, 2007.

[9] C. Satterfield, *Heterogeneous Catalysis in Practice*, McGraw-Hill, New York, NY, USA, 1980.

[10] L. Čapek, J. Adam, T. Grygar et al., "Oxidative dehydrogenation of ethane over vanadium supported on mesoporous materials of M41S family," *Applied Catalysis A: General*, vol. 342, no. 1-2, pp. 99–106, 2008.

[11] T. Blasco, A. Galli, J. M. López Nieto, and F. Trifiró, "Oxidative dehydrogenation of ethane and n-butane on VOx/Al_2O_3 catalysts," *Journal of Catalysis*, vol. 169, no. 1, pp. 203–211, 1997.

[12] G. Tsilomelekis, A. Christodoulakis, and S. Boghosian, "Support effects on structure and activity of molybdenum oxide catalysts for the oxidative dehydrogenation of ethane," *Catalysis Today*, vol. 127, no. 1–4, pp. 139–147, 2007.

[13] C. Liu and U. S. Ozkan, "Effect of chlorine on redox and adsorption characteristics of Mo/Si:Ti catalysts in the oxidative dehydrogenation of ethane," *Journal of Molecular Catalysis A: Chemical*, vol. 220, no. 1, pp. 53–65, 2004.

[14] A. Khodakov, B. Olthof, A. T. Bell, and E. Iglesia, "Structure and catalytic properties of supported vanadium oxides: support effects on oxidative dehydrogenation reactions," *Journal of Catalysis*, vol. 181, no. 2, pp. 205–216, 1999.

[15] A. Corma, J. M. L. Nieto, and N. Paredes, "Influence of the preparation methods of V-Mg-O catalysts on their catalytic properties for the oxidative dehydrogenation of propane," *Journal of Catalysis*, vol. 144, no. 2, pp. 425–438, 1993.

[16] P. Botella, A. Dejoz, J. M. L. Nieto, P. Concepción, and M. I. Vázquez, "Selective oxidative dehydrogenation of ethane over MoVSbO mixed oxide catalysts," *Applied Catalysis A: General*, vol. 298, no. 1-2, pp. 16–23, 2006.

[17] M. V. Martínez-Huerta, X. Gao, H. Tian, I. E. Wachs, J. L. G. Fierro, and M. A. Bañares, "Oxidative dehydrogenation of ethane to ethylene over alumina-supported vanadium oxide catalysts: relationship between molecular structures and chemical reactivity," *Catalysis Today*, vol. 118, no. 3-4, pp. 279–287, 2006.

[18] Z.-S. Chao and E. Ruckenstein, "Noncatalytic and catalytic conversion of ethane over V-Mg oxide catalysts prepared via solid reaction or mesoporous precursors," *Journal of Catalysis*, vol. 222, no. 1, pp. 17–31, 2004.

[19] R. B. Watson, S. L. Lashbrook, and U. S. Ozkan, "Chlorine modification of Mo/silica-titania mixed-oxide catalysts for the oxidative dehydrogenation of ethane," *Journal of Molecular Catalysis A: Chemical*, vol. 208, no. 1-2, pp. 233–244, 2004.

[20] R. B. Watson and U. S. Ozkan, "Mo loading effects over Mo/Si: Ti catalysts in the oxidative dehydrogenation of ethane," *Journal of Catalysis*, vol. 208, no. 1, pp. 124–138, 2002.

[21] G. Grubert, E. Kondratenko, S. Kolf, M. Baerns, P. Van Geem, and R. Parton, "Fundamental insights into the oxidative dehydrogenation of ethane to ethylene over catalytic materials discovered by an evolutionary approach," *Catalysis Today*, vol. 81, no. 3, pp. 337–345, 2003.

[22] C. Yokoyama, S. S. Bharadwaj, and L. D. Schmidt, "Platinum-tin and platinum-copper catalysts for autothermal oxidative dehydrogenation of ethane to ethylene," *Catalysis Letters*, vol. 38, no. 3-4, pp. 181–188, 1996.

[23] D. W. Flick and M. C. Huff, "Oxidative dehydrogenation of ethane over supported chromium oxide and Pt modified chromium oxide," *Applied Catalysis A: General*, vol. 187, no. 1, pp. 13–24, 1999.

[24] G. D. Claycomb, P. M. A. Sherwood, B. E. Traxel, and K. L. Hohn, "X-ray photoelectron spectroscopic study of the surface state during ethane oxidative dehydrogenation at millisecond contact times," *The Journal of Physical Chemistry C*, vol. 111, no. 50, pp. 18724–18730, 2007.

[25] E. A. de Graaf, G. Rothenberg, P. J. Kooyman, A. Andreini, and A. Bliek, "Pt0.02Sn0.003Mg0.06 on γ-alumina: a stable catalyst for oxidative dehydrogenation of ethane," *Applied Catalysis A: General*, vol. 278, no. 2, pp. 187–194, 2005.

[26] B. Solsona, A. Dejoz, T. Garcia et al., "Molybdenum-vanadium supported on mesoporous alumina catalysts for the oxidative dehydrogenation of ethane," *Catalysis Today*, vol. 117, no. 1-3, pp. 228–233, 2006.

[27] M. Roussel, M. Bouchard, K. Karim, S. Al-Sayari, and E. Bordes-Richard, "MoVO-based catalysts for the oxidation of ethane to ethylene and acetic acid: influence of niobium and/or palladium on physicochemical and catalytic properties," *Applied Catalysis A: General*, vol. 308, pp. 62–74, 2006.

[28] Q. Xie, L. Chen, W. Weng, and H. Wan, "Preparation of MoVTe(Sb)Nb mixed oxide catalysts using a slurry method for selective oxidative dehydrogenation of ethane," *Journal of Molecular Catalysis A: Chemical*, vol. 240, no. 1-2, pp. 191–196, 2005.

[29] D. Linke, D. Wolf, M. Baerns et al., "Catalytic partial oxidation of ethane to acetic acid over $Mo_1V_{0.25}Nb0.12Pd_{0.0005}O_x$: I. Catalyst performance and reaction mechanism," *Journal of Catalysis*, vol. 205, no. 1, pp. 16–31, 2002.

[30] D. Linke, D. Wolf, M. Baerns, S. Zeyß, U. Dingerdissen, and L. Mleczko, "Catalytic partial oxidation of ethane to acetic acid over $Mo_1V_{0.25}Nb_{0.12}$ $Pd_{0.0005}O_x$: reactor operation," *Chemical Engineering Science*, vol. 57, no. 1, pp. 39–51, 2002.

[31] D. Linke, D. Wolf, M. Baerns, S. Zeyß, and U. Dingerdissen, "Catalytic partial oxidation of ethane to acetic acid over $Mo_1V_{0.25}Nb_{0.12}Pd_{0.0005}O_x$: II. Kinetic modelling," *Journal of Catalysis*, vol. 205, no. 1, pp. 32–43, 2002.

[32] E. M. Thorsteinson, T. P. Wilson, F. G. Young, and P. H. Kasai, "The oxidative dehydrogenation of ethane over catalysts containing mixed oxides of molybdenum and vanadium," *Journal of Catalysis*, vol. 52, no. 1, pp. 116–132, 1978.

[33] X. Lin, K. R. Poeppelmeier, and E. Weitz, "Oxidative dehydrogenation of ethane with oxygen catalyzed by K-Y zeolite supported first-row transition metals," *Applied Catalysis A: General*, vol. 381, no. 1-2, pp. 114–120, 2010.

[34] D. Vitry, Y. Morikawa, J. L. Dubois, and W. Ueda, "Mo-V-Te-(Nb)-O mixed metal oxides prepared by hydrothermal synthesis for catalytic selective oxidations of propane and propene to acrylic acid," *Applied Catalysis A: General*, vol. 251, no. 2, pp. 411–424, 2003.

[35] K. Karim, A. Mamedov, M. H. Al-Hazmi, and N. Al-Andis, "Oxidative dehydrogenation of ethane over MoVMnW oxide catalysts," *Reaction Kinetics and Catalysis Letters*, vol. 80, no. 1, pp. 3–11, 2003.

[36] K. S. Karim, M. H. Al-Hazmi, and N. Al-Andis, "Catalysts for oxidative dehydrogenation of ethane," *Arabian Journal for Science and Engineering*, vol. 24, no. 1, pp. 41–48, 1999.

[37] J. Tichý, "Oxidation of acrolein to acrylic acid over vanadium-molybdenum oxide catalysts," *Applied Catalysis A: General*, vol. 157, no. 1-2, pp. 363–385, 1997.

[38] T. Blasco, J. M. L. Nieto, A. Dejoz, and M. I. Vazquez, "Influence of the acid-base character of supported vanadium catalysts on their catalytic properties for the oxidative dehydrogenation of *n*-butane," *Journal of Catalysis*, vol. 157, no. 2, pp. 271–282, 1995.

[39] A. Dejoz, J. M. López Nieto, F. Márquez, and M. I. Vázquez, "The role of molybdenum in Mo-doped V-Mg-O catalysts during the oxidative dehydrogenation of *n*-butane," *Applied Catalysis A: General*, vol. 180, no. 1-2, pp. 83–94, 1999.

[40] J. Guan, H. Xu, K. Song et al., "Selective oxidation and oxidative dehydrogenation of isobutane over hydrothermally synthesized Mo-V-O mixed oxide catalysts," *Catalysis Letters*, vol. 126, no. 3-4, pp. 293–300, 2008.

[41] E. R. Stobbe, B. A. de Boer, and J. W. Geus, "The reduction and oxidation behaviour of manganese oxides," *Catalysis Today*, vol. 47, no. 1–4, pp. 161–167, 1999.

[42] B. Solsona, J. M. López Nieto, P. Concepción, A. Dejoz, F. Ivars, and M. I. Vázquez, "Oxidative dehydrogenation of ethane over Ni-W-O mixed metal oxide catalysts," *Journal of Catalysis*, vol. 280, no. 1, pp. 28–39, 2011.

[43] P. Botella, E. García-González, A. Dejoz, J. M. López Nieto, M. I. Vázquez, and J. González-Calbet, "Selective oxidative dehydrogenation of ethane on MoVTeNbO mixed metal oxide catalysts," *Journal of Catalysis*, vol. 225, no. 2, pp. 428–438, 2004.

[44] M. D. Argyle, K. Chen, A. T. Bell, and E. Iglesia, "Ethane oxidative dehydrogenation pathways on vanadium oxide catalysts," *Journal of Physical Chemistry B*, vol. 106, no. 21, pp. 5421–5427, 2002.

[45] S. Al-Khattaf, J. A. Atias, K. Jarosch, and H. de Lasa, "Diffusion and catalytic cracking of 1,3,5 tri-iso-propyl-benzene in FCC catalysts," *Chemical Engineering Science*, vol. 57, no. 22-23, pp. 4909–4920, 2002.

[46] A. Voorhies, "Carbon formation in catalytic cracking," *Industrial & Engineering Chemistry*, vol. 37, no. 4, pp. 318–322, 1945.

[47] A. K. Agarwal and M. L. Brisk, "Sequential experimental design for precise parameter estimation. 1. Use of reparameterization," *Industrial & Engineering Chemistry Process Design and Development*, vol. 24, pp. 203–207, 1986.

[48] Y. Choi and P. Liu, "Mechanism of ethanol synthesis from syngas on Rh(111)," *Journal of the American Chemical Society*, vol. 131, no. 36, pp. 13054–13061, 2009.

[49] Y. Choi and P. Liu, "Understanding of ethanol decomposition on Rh(1 1 1) from density functional theory and kinetic Monte Carlo simulations," *Catalysis Today*, vol. 165, no. 1, pp. 64–70, 2011.